

www.acsnano.org

Multipurpose and Reusable Ultrathin Electronic Tattoos Based on PtSe₂ and PtTe₂

Dmitry Kireev,* Emmanuel Okogbue, RT Jayanth, Tae-Jun Ko, Yeonwoong Jung, and Deji Akinwande



Cite This: ACS Nano 2021, 15, 2800-2811



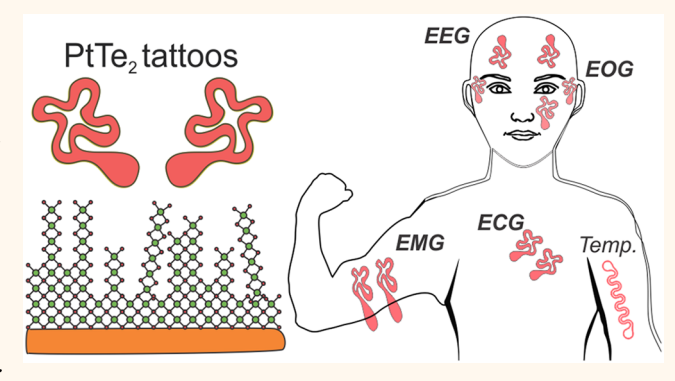
ACCESS I

Metrics & More



Supporting Information

ABSTRACT: Wearable bioelectronics with emphasis on the research and development of advanced person-oriented biomedical devices have attracted immense interest in the past decade. Scientists and clinicians find it essential to utilize skin-worn smart tattoos for on-demand and ambulatory monitoring of an individual's vital signs. Here, we report on the development of ultrathin platinum-based two-dimensional dichalcogenide (Pt-TMDs)-based electronic tattoos as advanced building blocks of future wearable bioelectronics. We made these ultrathin electronic tattoos out of large-scale synthesized platinum diselenide (PtSe₂) and platinum ditelluride (PtTe₂) layered materials and used them for monitoring human physiological vital signs, such as the electrical activity of



the heart and the brain, muscle contractions, eye movements, and temperature. We show that both materials can be used for these applications; yet, PtTe₂ was found to be the most suitable choice due to its metallic structure. In terms of sheet resistance, skin contact, and electrochemical impedance, PtTe₂ outperforms state-of-the-art gold and graphene electronic tattoos and performs on par with medical-grade Ag/AgCl gel electrodes. The PtTe₂ tattoos show 4 times lower impedance and almost 100 times lower sheet resistance compared to monolayer graphene tattoos. One of the possible prompt implications of this work is perhaps in the development of advanced human—machine interfaces. To display the application, we built a multitattoo system that can easily distinguish eye movement and identify the direction of an individual's sight.

KEYWORDS: epidermal electronics, 2D materials, wearable electronics, lab-on-skin, healthcare monitoring, electro-oculography, bioelectronics

tomically thin layered materials have recently emerged as an entirely distinct class of materials with advanced, peculiar, and often unexpected properties. Transition metal dichalcogenides (TMDs), with a generic MX₂ composition, are perhaps the most well studied of these two-dimensional materials, beyond graphene, up to date.2 Changing the constituents of M and X in certain combinations is allowed where M is a transition metal (e.g., Mo, W, Pt, V, etc.) and X is a chalcogen (S, Se, Te). While most of the TMDs known to date are semiconducting or metallic, they are found to possess a plurality of other properties for realizing fully 2D-based electronic devices with an entirely different set of properties. The layered structure associated with TMDs is of particular interest, and the electronic properties vary drastically from bulk to multi- and single-layered materials.^{3,4} Imperceptible thickness, typically in the range of 1 nm of a monolayer 2D material, makes it intrinsically flexible, yet soft and adaptable, allowing it to conform to arbitrary shapes. 5 This allows the 2D materials to establish very firm and reliable, yet soft, contact to soft and squishy biological tissue without affecting its properties. In

contrast to the hard and rigid silicon-based technology or any other bulk material, whose elements are not exactly compatible with biological tissue due to mechanical mismatch, 2D materials bring essential advancement to the field. Typically, the single atomic layers of 2D materials are highly transparent in the visible wavelength region (97% transparency in the case of graphene). The above-mentioned electrical, optical, and mechanical properties of the 2D TMDs make them generally attractive as fundamental components of future wearable bioelectronics.

Platinum is one of the most stable metals from the group 10 materials and is considered a noble metal (along with gold). It is well-known for its resistance to corrosion, 8 catalytic properties, 9

Received: October 17, 2020 Accepted: January 11, 2021 Published: January 20, 2021





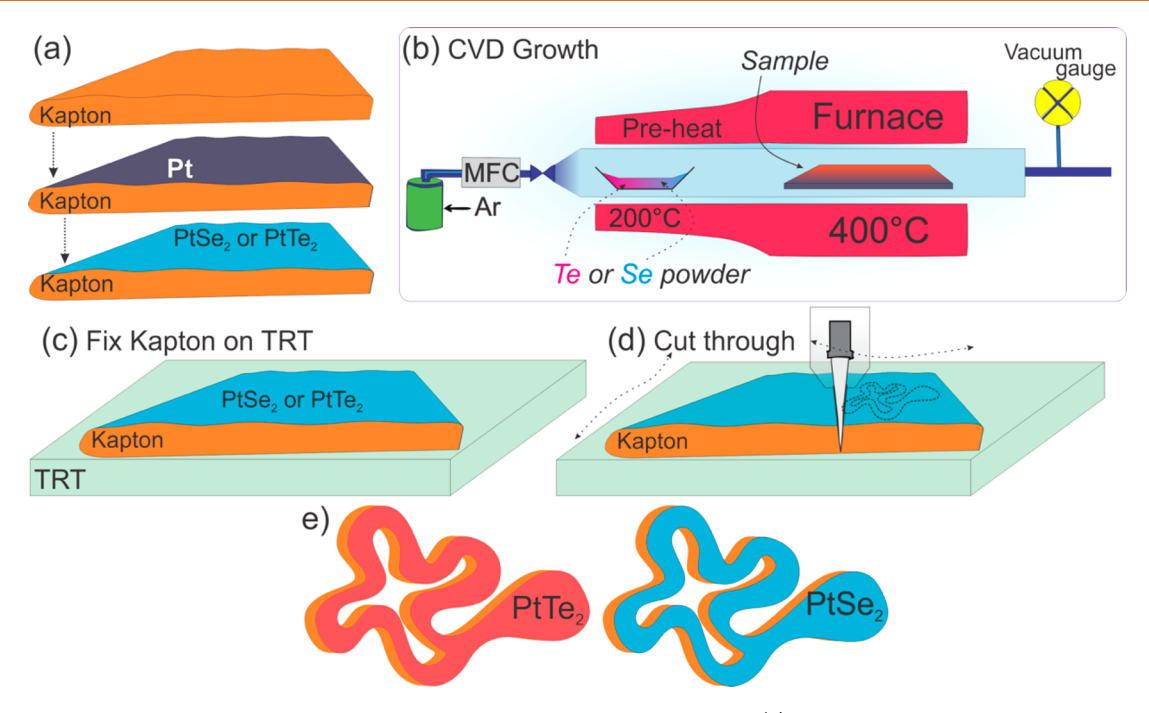


Figure 1. Schematic overview of Kapton-based Pt-TMD tattoo design and fabrication flow. (a) Evaporation of thin Pt on top of the Kapton film, followed by TAC conversion into Pt-TMD. (b) Schematic of the TAC CVD process. (c) Post-CVD growth, the Pt-TMD/Kapton sample is fixed on top of a TRT. (d) Mechanical patterning process of the Pt-TMDs grown on Kapton film. (e) Schematics of the final PtSe₂ and PtTe₂ tattoos supported by Kapton.

and biocompatibility.¹⁰ Pt is frequently used in fundamental research and industrial applications as an electrode, catalyst, *etc.* Consequently, Pt-based TMDs (Pt-TMDs) were theoretically expected and have since been proven experimentally to have good air and water stability,¹¹ compared to that with other TMDs. Pt-TMDs typically feature thickness-dependent semiconductor-to-metal transition,^{4,12} ambient stability,¹¹ and low synthesis temperature.^{13–15} Such properties position them as top candidates for the development of wearable bioelectronic devices.

Out of the different Pt-TMDs, two have recently attracted immense interest owing to their distinctive thickness-mediated change in electronic properties: platinum diselenide (PtSe₂) and platinum ditelluride (PtTe₂). Monolayer PtSe₂ is a semiconductor with an indirect band gap of 1.25 eV, which transforms into a metallic character with an increased number of layers. PtTe₂, however, has a stronger interaction between the interlayer chalcogen atoms (Te), making the out-of-plane valence bond broader and overlapping, leading to its increased metallic properties even with small layer numbers. Consequently, PtTe₂ has metallic properties. Consequently, PtTe₂ has metallic properties.

An advantage of PtSe₂ and PtTe₂ compared to other TMDs is their low-temperature growth requirements. The thermal-assisted conversion method allows for the growth of high-quality PtSe₂^{4,13,15} and PtTe₂^{19,20} films on a large scale and at temperatures as low as 400 °C, making it compatible with polymeric substrates. ¹⁴ The direct growth of 2D TMDs on ultrathin polyimide allows the fabrication of flexible materials with promising bioelectronic properties that have high prospects of being the future building blocks of next-generation wearable devices. PtSe₂ and PtTe₂ are considered promising for numerous bioelectronic applications, yet none has been practically realized so far. Biocompatibility of the PtSe₂ and PtTe₂ material has been evaluated previously²¹ showing that both Pt-TMDs in flake form have superior properties compared to the more common Pt/C

due to the synergistic effect of platinum bonded to chalcogens, hence reducing the toxicity level of the materials. In large-scale, polymer-supported form, the Pt-TMDs are expected to have little to no cytotoxicity.

In this present work, we show how PtSe2 and PtTe2 can be used to develop multipurpose and reusable electronic tattoos with diverse bioelectronics applications. In terms of electrical conductivity, skin contact, and electrochemical impedance, PtTe₂ outperforms graphene electronic tattoos²² and performs on par or even better than classical Ag/AgCl gel electrodes (despite the ~12 times smaller area). Skin-impedance-based electrode characterization data are supplemented with the electrical impedance spectroscopy (EIS) measurements, both suggesting that ultrathin PtTe₂ is a promising material to be used as an electrode for future bio- and neuro-interfaces. In the present work, we showcase several applications of Pt-TMDs for numerous wearable healthcare applications. One of them is measuring electromyograms (EMG, muscle contractions) for building next-generation human-machine interfaces. Recording electro-oculograms (EOG), eye-movement-related electrical activity, is demonstrated as the prototype application for the imperceptible skin-worn electronic tattoos. By placing electrodes on the top, bottom, and to the sides of a subject's eye, we built a soft and ultrathin interface that can capture eye movements, hence, it can be further used for robotic interfaces. Continuous and fault-free monitoring of electrocardiogram (ECG, heartbeat) and electroencephalogram (EEG, brainwaves) is an essential aspect of hospital-based biopotential monitoring systems. Here, we performed these same tasks with PtTe2 and PtSe2 tattoos, showing their applicability for personalized and mobile healthcare. Body temperature monitoring is another example of an essential vital biomarker. We have found experimentally that the body temperature can be precisely monitored utilizing PtSe₂ and PtTe₂ sensors that show opposite signs in the measured temperature electrical coefficient (TEC).

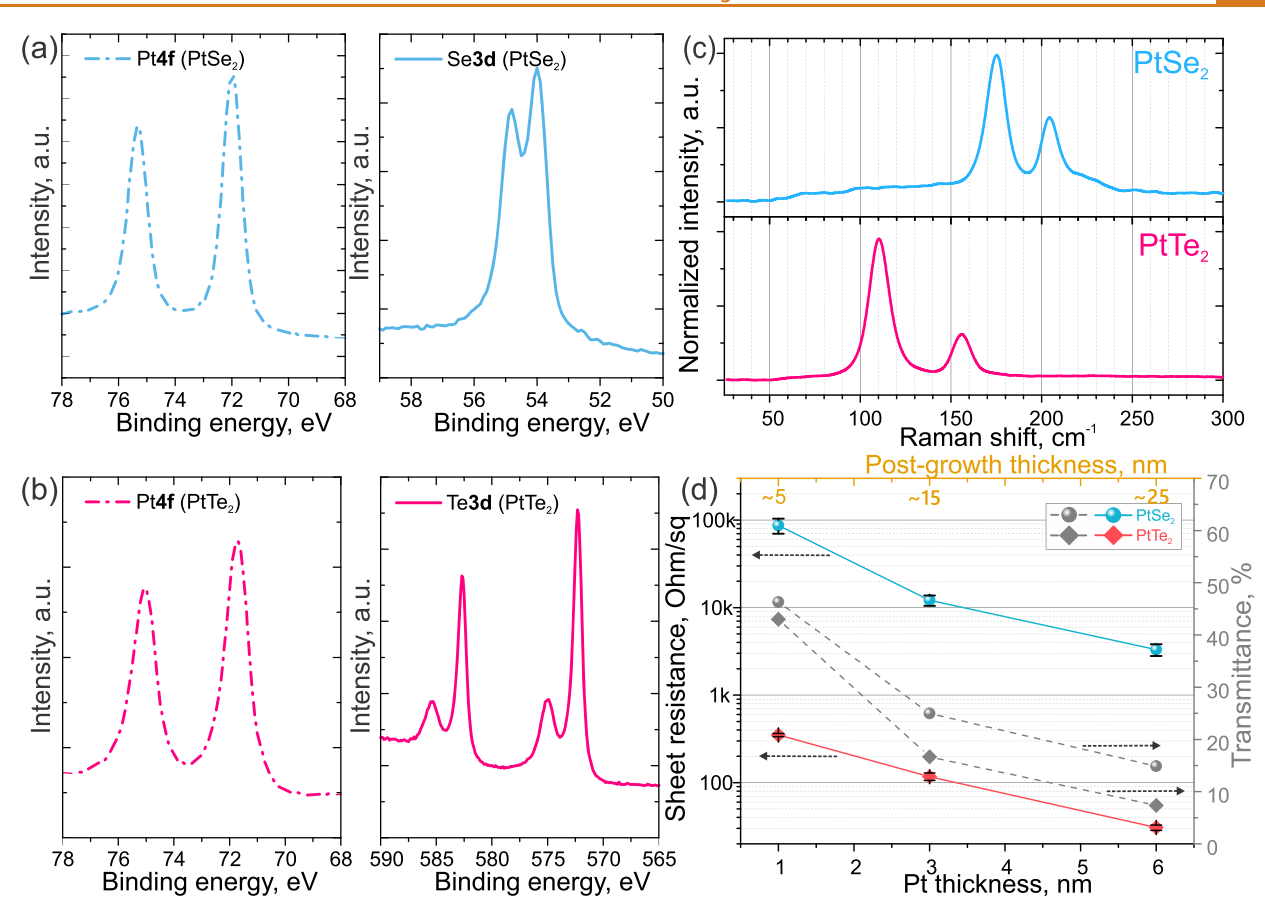


Figure 2. (a) XPS characterization of Pt 4f and Se 3d core levels obtained from PtSe₂ layers on SiO₂/Si substrates. (b) XPS characterization of Pt 4f and Te 3d core levels obtained from PtTe₂ layers on SiO₂/Si substrates. (c) Raman spectra of as-grown PtSe₂ and PtTe₂ layers. (d) Sheet resistance and optical transmittance (at 550 nm) of PtSe₂ and PtTe₂ as a function of its thickness, pregrowth, and postgrowth.

RESULTS AND DISCUSSION

PtSe2 and PtTe2 used in this work are grown by a thermalassisted conversion (TAC)-based chemical vapor deposition (CVD) process. The growth is performed at moderately low temperatures, at about 400 °C, allowing us to grow the material directly on top of select polymers. 14 A classic temperature-stable polymer commonly used in bioelectronic applications is Kapton, known for its mechanical and temperature stability. In this work, we use two kinds of Pt-TMD tattoos: some are grown directly over Kapton, others are grown on SiO₂/Si wafers and then transferred onto an ultrathin temporary tattoo form utilizing mechanical support of a 200 nm thick poly(methyl methacrylate) (PMMA) layer. 22 The TAC process requires platinum to be predeposited on the samples' surface (see Figure 1a and Figure S1a). We use 6 nm thick Pt as the material source for Kapton structures and 3 nm thick Pt as the source for SiO₂/Si growth material. The 6 nm thick Pt samples, post-CVD growth, result in \sim 25 \pm 3 nm thick multilayer Pt-TMD that features multiple out-of-plane growth planes (see Supporting Information for details). The 3 nm thick samples typically result in \sim 15 ± 3 nm thick layered dichalcogenide, with a more uniform inplane layered arrangement, which has been deemed beneficial for PMMA-supported tattoo material. After the CVD growth is performed (Figure 1b), the Kapton-based samples are ready for final processing. In contrast, the Si-based ones require further additional transfer steps (see Methods for details). The PMMAand Kapton-based Pt-TMD tattoos are finally cut into desired shapes by means of a cutter-plotter tool (Silhouette Cameo).

The PMMA-based tattoos are just slightly scribed, while the Kapton-based samples are cut through their thickness. The Kapton samples are also fixed onto thermal release tape (TRT) to allow precise and fault-free cutting (see Figure 1c,d). The final devices are of arbitrary shape and either supported by a 25 μ m thick Kapton or a 200 nm thick PMMA (Figure 1e and Figure S1i).

To confirm the quality of the as-grown PtSe₂ and PtTe₂ layers, we carried out structural characterization employing X-ray photoelectron spectroscopy (XPS) and Raman spectroscopy. Figure 2a shows the Pt 4f and Se 3d core-level spectra obtained from the Pt-deposited substrates after undergoing thermalassisted conversion to PtSe₂ layers in the CVD furnace. The Pt 4f spectra show no elemental Pt signal, indicating that the entire spectrum can be assigned to Pt⁴⁺ that corresponds to PtSe₂. Similarly, the Se 3d spectra represent PtSe₂ whose spin-up state (j = 2 + 1/2) is located at ~ 54 eV. ¹⁴ The XPS profile in Figure 2b (left) shows the core-level peaks of Pt 4f at \sim 72.2 and \sim 75.1 eV assigned to the doublet $4f_{7/2}$ and $4f_{5/2}$ of PtTe₂. The XPS profile reported in Figure 2b (right) shows the Te 3d core-level spectra with peaks at \sim 576 and \sim 586 eV that correspond to the Te (IV) species as well as the additional peaks at \sim 572.6 and \sim 582.9 eV, corresponding to Te (0). The peaks obtained from the Pt 4f and Te 3d core-level spectra of PtTe2 are also consistent with previous reports.²³ Additionally, Raman spectra were collected from the PtTe2 and PtSe2 layers directly grown on SiO2/Si substrates. The Raman profiles in Figure 2c show two distinct peaks corresponding to vibration modes for PtSe₂ and PtTe₂ layers. The PtSe₂ samples exhibit two dominant peaks; E_{\sigma} mode

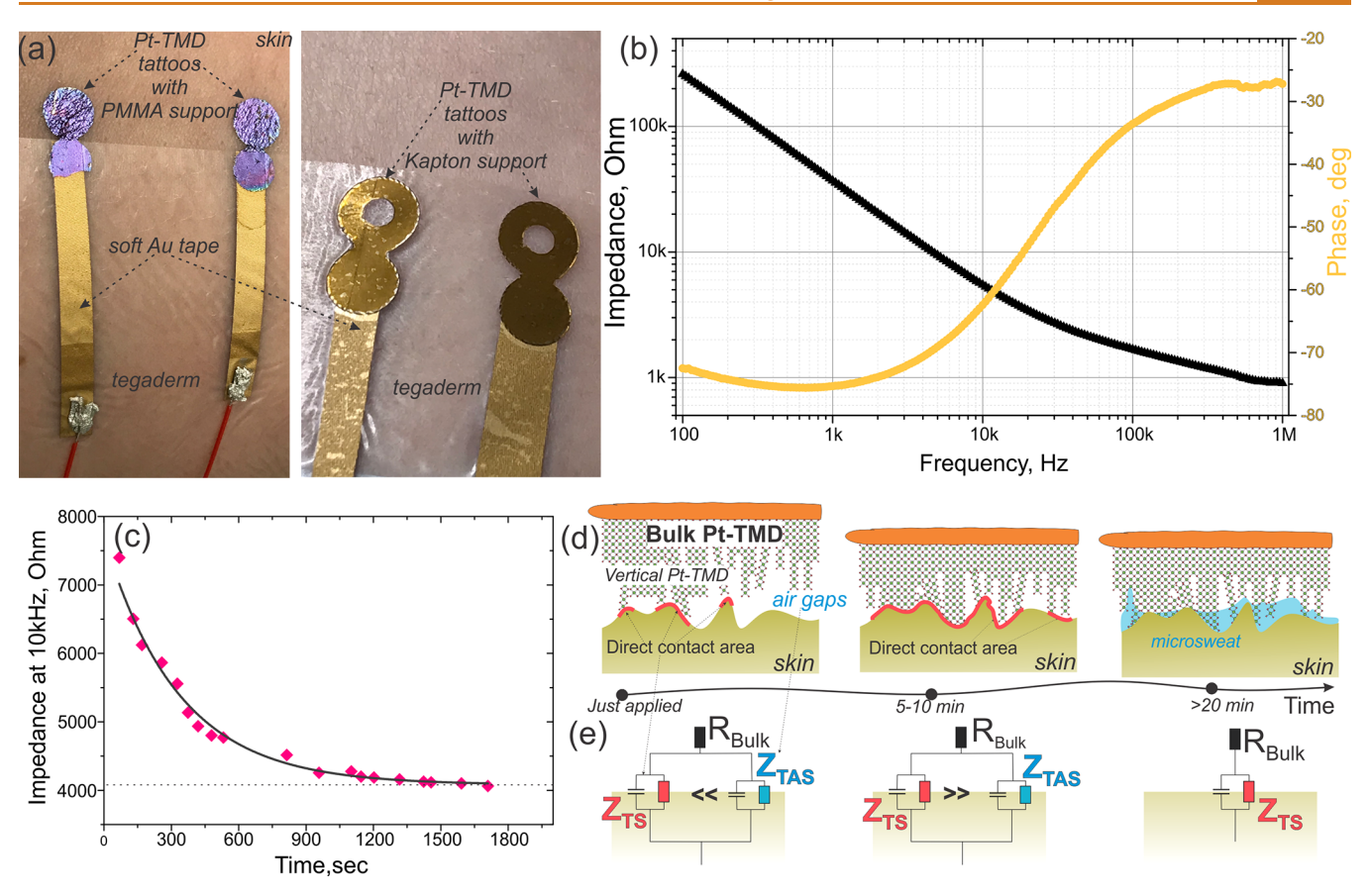


Figure 3. (a) Pictures of Pt-TMD tattoos, with PMMA (left) and Kapton (right) polymeric support and built-up electrical contacts. (b) Typical Bode diagram of the PtTe $_2$ -skin impedance. (c) Temporal exponential decay of the contact impedance (at 10 kHz) upon applying PtTe $_2$ tattoos on the skin. (d—e) Proposed schematic of the time-related dynamic changes to Pt-TMD-skin interface with suggested equivalent circuits. $Z_{\rm TS}$ and $Z_{\rm TAS}$ represent direct tattoo-skin and indirect tattoo-air-skin complex impedances, respectively.

at 175 cm $^{-1}$ and A_{1g} mode at 205 cm $^{-1}$ correspond to the inplane and out-of-plane vibration motions of the Se atoms, respectively. Similarly, the Raman spectra collected from PtTe $_2$ show peaks at $\sim\!110$ and 157 cm $^{-1}$ correspond to E_g and A_{1g} modes. 25,26

As one can see from the photographs (e.g., Figure 3a and Figure S17), the tattoos are not entirely transparent. This is mainly due to the number of TMD layers, and the optical transparency can be greatly improved if TMDs of smaller thickness are used. Having confirmed the growth of PtSe2 and PtTe2 layers, we investigated the thickness-dependent optical properties using UV-Vis spectroscopy. Figure 2d shows the optical transmittance (at 550 nm) along with sheet resistance and of the PtSe₂ and PtTe₂ layers with respect to the material's thickness (see Figures S3 and S4 for the full data set). PtSe₂ films become more semiconducting as the thickness decreases, according to recent reports on PtSe2-based electrical devices. 15,27 The corresponding sheet resistance of the PtSe2 layers decrease from ${\sim}100$ to ${\sim}1~\text{k}\Omega/{\textstyle\square}$ as the thickness increases. In contrast to PtSe₂ films, PtTe₂ films retain their metallic transport properties at varying thickness, which is in accordance with recent reports. 26,28 The sheet resistance of PtTe₂ ranges from \sim 350 Ω/\square at 1 nm, down to as low as \sim 31 Ω/\square at 6 nm. PtSe₂ and PtTe2 layers with a Pt seed layer thickness of ~1 nm have optical transmittance of ~50%, with a noticeable increase in the optical absorbance with increased thickness, similar to the observation in other 2D TMDs. The multilayered PtSe2 and PtTe₂ materials used in this study remain ultrathin with a

postgrowth thickness of less than 30 nm (see Figure S4 for details).

Once fabricated, both kinds of tattoos can be easily placed on the skin for characterization and electrophysiology. The temporary tattoo electrodes, supported by the PMMA, are transferred similarly to the graphene electronic tattoos²² (see Supplementary Video S3). PMMA provides a more imperceptible and intimate contact with the skin. As can be seen from the Supplementary Video S1, the tattoos come in a very secure contact with the skin, surviving motion, bending, and stretching. On the other hand, the Kapton-based structures can be simply held in place *via* a piece of Tegaderm or kind removal silicone tape (KRST), making them reusable. Pictures of both types of Pt-TMD tattoos supported by PMMA and Kapton on skin are shown in Figure 3a and Figure S17.

To examine the electrode-to-skin impedance of Pt-TMDs and compare them to the state-of-the-art, we fabricated tattoos made of bare platinum, bare gold, PtSe₂, and PtTe₂ over Kapton substrates. The Kapton-supported Pt-TMD electronic tattoos provide electronic properties superior to those of PMMA-supported ones; hence they have been used for a majority of the following studies, including skin impedance, electrochemical impedance tests, and all electrophysiological data monitoring. The tattoos were manufactured as explained above, with at least five pairs of each kind used to study the electrode—skin impedance. Graphene tattoos were fabricated as explained elsewhere. Considering that the actual tissue impedance is in the range of several hundreds of m Ω to dozens of Ω , ²⁹ the skin

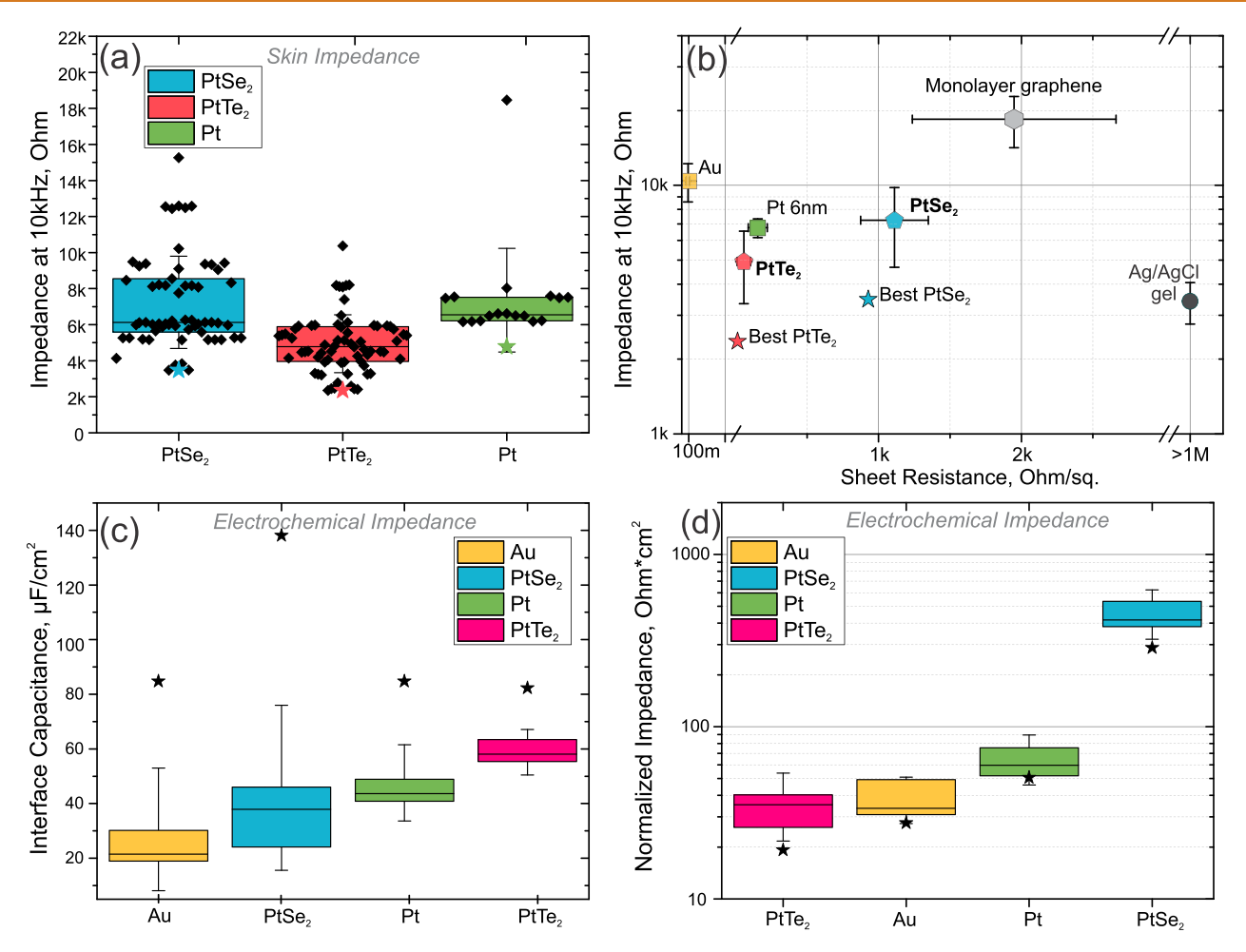


Figure 4. (a) Statistical distribution of the electrode-skin impedance values for $PtSe_2$ (6 nm, blue), $PtTe_2$ (6 nm, pink), and bare Pt (6 nm, green). (b) Comparison scatter graph of both skin impedance and sheet resistance of Au (100 nm, yellow), Pt (6 nm, green), $PtTe_2$ and $PtSe_2$, monolayer graphene tattoos (light gray), and $PtSe_2$, and $PtSe_2$, monolayer graphene tattoos (light gray), and $PtSe_2$, $PtSe_2$ (ark gray). Impedance is reported at 10 kHz frequency and is averaged from $PtSe_2$ electrodes. The sheet resistance is averaged from $PtSe_2$ (ark gray). Impedance and different devices. (c,d) Electrochemical impedance spectroscopy data of the PtTMD's interface capacitance and normalized impedance (at 1 kHz) correspondingly. In (a,c,d), the box represents 25 and 75% with a mean, outliers are $ptSe_2$ and stars represent the best examples.

impedance value measured between the electrode pair placed over the skin will give us the electrode—skin impedance. This property is commonly considered as a figure-of-merit of the wearable electrodes. ^{30–32} A typical Pt-TMD—skin impedance plot can be seen in Figure 3b, featuring the regular 1/f frequency dependency. The common figure-of-merit of skin—electrode impedance is the value at 10 kHz, at the frequency the current passes through both intra- and extracellular fluids, hence providing most complete representation of the tissue impedance. Moreover, 10 kHz is a common frequency used in wearable electronic devices that feature current injection, as higher current magnitudes can be safely injected into the tissue at higher frequencies. ³³

A peculiar dynamics was observed for the case of Pt-TMD-based tattoos, on which, just upon placement onto the skin, the electrodes feature relatively high impedance (\sim 10 k Ω @10 kHz) that rapidly decreases over a time period of about 15 min to reach a steady-state value of \sim 4 k Ω (Figure 3c). We believe this might be related to the structural properties of the thick Pt-TMDs. As reported (and confirmed via high-resolution transmission electron microscopy imaging) previously, CVD growth of thicker (>6 nm seed layer) Pt-TMDs results in domains of vertically aligned layers exposing their 2D edge sites

on the surface (see Figure 3d). 15,20,34 This would result in uneven height distribution and nanoscale rough surface on the material. When placed onto the skin, the rough nanosurface of Pt-TMDs in combination with the microporous structure of skin results in a high-impedance condition due to the presence of trapped air, reducing the overall direct contact area. Over time, the tattoos forge a more intimate contact with skin, reducing the air gaps, and establishing a closer connection. Moreover, we hypothesize that upon certain conditions (e.g., when Tegaderm fixes the Kapton-based tattoos), the macroscopic sweat and moisture gets trapped between the skin and Pt-TMD, further improving the contact impedance.³⁰ To corroborate this hypothesis, we performed curve fitting of the frequencydependent impedance data measured over time upon application over the skin (20 points, with ~90 s intervals). As given in Figure 3e, the proposed equivalent circuits are impossible to fit as the number of variables is too large, and the model can converge at any arbitrary value. However, upon fitting the impedance with a simple Randles circuit³⁵ (see Figure S5), the resulting fit is profoundly unstable in the first 900 s after tattoo application but yields relevant and reliable values after 900 s. The results indicate that the simplified Randles circuit with low ohmic access resistance ($<400 \Omega$), low contact

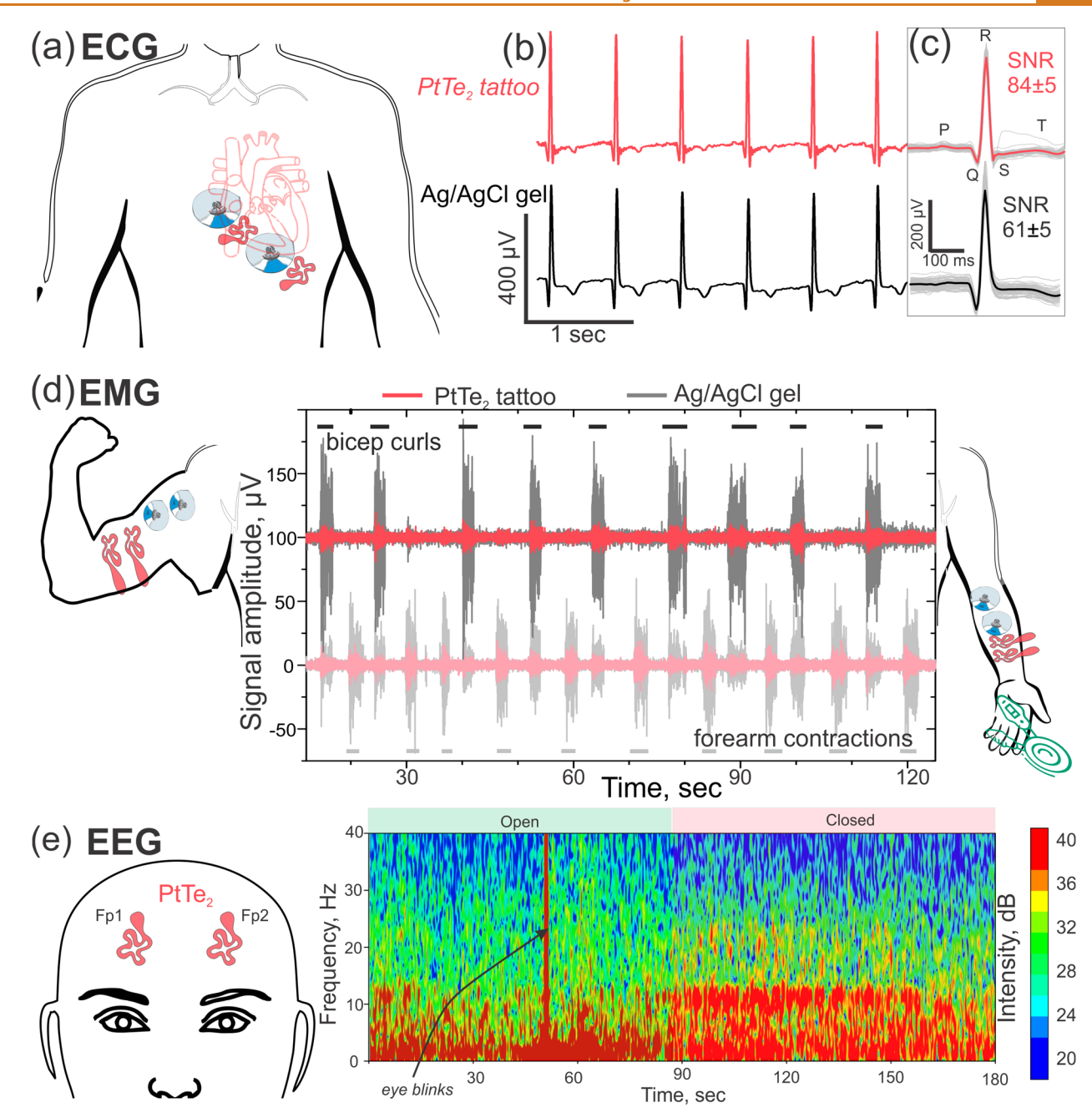


Figure 5. Wearable electrophysiological recordings with Pt-TMDs. (a) Schematic of the electrode placement for the ECG measurement. (b) Five-second-long ECG timetrace from PtTe₂ tattoos and Ag/AgCl gel electrodes. (c) Average ECG signal shapes, amplitudes, and average SNRs for PtTe₂ tattoo and Ag/AgCl gel electrode. (d) Schematic of electrode placement and EMG recordings from a human's bicep (top) and forearm (bottom) muscle contractions recorded *via* the Ag/Ag gel electrodes and PtTe₂ tattoos simultaneously. The horizontal bars on the top and bottom mark the events and durations of the bicep curls and forearm contractions correspondingly. (e) Electrode placement for EEG measurements (left) and resulting spectrogram (right) from one of the PtTe₂ tattoos placed on the Fp1 and Fp2 locations on the subject's forehead.

resistance (\sim 200 k Ω), imperfect (a=0.85) capacitor, and a constant phase element (CPE, \sim 8.5 nF) is a reasonable estimation of the interface after \sim 900 s upon tattoo application but is a poor estimation of the interface during the initial transitory contact-forming stage. To show durability and reusability of the reported Pt-TMD tattoos, two experiments were performed. First, the tattoo pairs were placed onto the subject's forearm for a measurement, then peeled off, placed back on, with \sim 20 min intervals, and repeated for 24 h. In the other experiment, the tattoos were kept constantly on a subject's bicep for 24 h. Both results (see Figures S18 and S19) show that

tattoo performance does not degrade but rather improves from long-term intimate contact with skin.

To ensure that the figure-of-merit values of Pt-TMD-to-skin impedance are most representative, we let the tattoos stay on the skin for at least 20 min before performing the measurements. Multiple batches of Pt-TMDs were utilized in order to make sure that the data reported represent the median material behavior and not a random sample. At least four pairs (N > 8) of each tattoo kind were used to gather the statistically relevant data. The impedance (at $10 \, \text{kHz}$) distribution of the PtSe₂, PtTe₂, and Pt samples is shown in Figure 4a. It is clear from the figure and

the numbers that the PtTe₂ offers the lowest impedance, averaging $4.94 \pm 1.61 \text{ k}\Omega$. PtSe₂, in comparison, averages at 7.24 \pm 2.56 k Ω , which is slightly worse than bare Pt with 6.75 \pm 0.59 $k\Omega$. The full statistical distribution of the electrode-skin impedance values for PtSe₂ and PtTe₂ is given in Figure S6. Electrode dimension is an important parameter to keep in mind since the classical electrical circuit model states that the electrode-skin impedance is inversely proportional to the electrode's area.³⁶ Therefore, all electrodes utilized in this work (except the Ag/AgCl gel ones) are made with a total area of 25 mm². The Ag/AgCl electrodes cannot be cut smaller, and hence we have trimmed them down to only ~100 mm² for electrode skin measurements. Still, they are kept at their original size of \sim 300 mm² for most of the electrophysiological measurements. Regardless of such 4-fold difference in surface area, some of the highest quality PtTe2 tattoos have shown better performance than the medical-grade Ag/AgCl gel electrodes. The sheet resistance of polymer-supported Pt-TMDs was measured by placing a strip of the material out of the same growth batch onto the Ecoflex-covered glass with four soft conductive gold electrodes. Ecoflex is used here to reproduce skin-like texture and softness. The 4-point transfer length measurement (TLM) was performed to estimate sheet resistance. The values reported are averages from at least 2-3 strips of each kind. The sheet resistance of PtTe₂ tattoos is impressively low, averaging at 56 ± 49 Ω/\Box , with the best-reported value of only 13 Ω/\Box . In comparison, PtSe₂ tattoos hit about $1.11 \pm 2.37 \text{ k}\Omega/\square$, which is almost 20 times higher. This can be attributed to the different nature of these two 2D materials: PtTe₂ is highly metallic, whereas PtSe₂, even in its bulk form, is semimetallic.

The overall plot of merit that combines sheet resistance and skin impedance data for PtSe₂, PtTe₂, Pt, gold, Ag/AgCl, and even monolayer graphene for comparison is shown in Figure 4b. The major trend noticeable from the plot is that PtTe₂ is much more promising for wearable applications than PtSe₂. Both PtSe₂ and PtTe₂ yield better skin impedance than bare Pt. PtTe₂ outperforms almost every other competitor material, including bare gold, and is on par with the medical-grade Ag/AgCl electrodes. Significantly, both PtSe₂ and PtTe₂ outperform monolayer graphene tattoos in terms of both electrical properties, which is an important improvement, considering that graphene tattoos typically feature an advanced adhesion to skin. ^{22,37}

To supplement and corroborate the skin impedance values, we have performed an EIS study of these materials. For EIS experiments, the Kapton-supported TMD tattoos and control samples were made with varied areas to achieve scalable results. The EIS measurements were taken in a three-electrode configuration; see details in the Methods section. Once measured, the EIS data were evaluated and fitted with an equivalent circuit, extracting the interface capacitance, and the electrode impedance (at 1 kHz). Here, we report the EIS values at 1 kHz as it is the most well-adapted frequency used as figureof-merit comparing microelectrode array systems.³⁸ The areanormalized interface capacitance and area-normalized electrode impedance of PtSe₂, PtTe₂, Au, and Pt are shown in Figure 4c,d. Similar to the skin impedance, PtTe₂ exhibits the most outstanding performance, featuring notably high interface capacitance of 62.2 \pm 8.2 μ F/cm² and smallest normalized impedance at 1 kHz of 35.4 \pm 18.6 Ω ·cm.² PtSe₂, as expected, shows a lower interface capacitance of 45.8 \pm 30.2 μ F/cm² and higher normalized impedance at 1 kHz of 472 \pm 151 Ω ·cm. To put these values in perspective, the normalized impedance at 1

kHz of monolayer graphene averages at $74 \pm 173~\Omega \cdot \text{cm}$, which is much higher than that of PtTe₂. The high interface capacitance and small normalized impedance are typically good signs of a material's performance and its usability for building advanced microelectrode arrays (MEAs) for *in vitro* and *in vivo* applications. It is essential to mention here that the electrodes used for EIS in this work are macrosized compared to microsized electrodes typically used in MEAs. We expect the overall interface capacitance of the microsized Pt-TMDs to improve when scaled down to microsized MEAs. Furthermore, considering the 2D nature of PtTe₂, its flexibility, and stability, it is certainly a suitable bioelectronic material, and we expect the works of PtTe₂-based MEAs or *in vivo* probes to follow soon.

To begin with the electrophysiological measurements, TMD tattoos were laminated on a subject's chest to measure ECG. At this moment and further, all electrophysiological measurements were performed by means of a simple off-the-shelf open-source board—Ganglion from OpenBCI. In the case of ECG recordings, one pair of Pt-TMD tattoos were placed on the chest, as schematically shown in Figure 5a. Another couple of Ag/AgCl gel electrodes were placed nearby with similar spacing to provide a direct signal comparison (see Figure 5a). A reference grounddriven electrode was placed over the lower right of the abdomen. The signals were sampled at 200 Hz and later filtered with a 60 Hz notch filter to remove the power line noise. The ECG signals measured with Ag/AgCl and PtTe2 are shown in Figure 5b,c with clearly present characteristic ECG peaks (P, Q, R, S, T). The signal-to-noise ratio (SNR) of PtTe₂ tattoo-based recordings was as high as 84 ± 6 , while the nearby Ag/AgCl gel electrodes yielded 61 \pm 5. Similar ECG signal recordings with the PtSe₂ tattoos are also shown in Figure S7. PtSe₂ tattoos' performance is slightly lower, yet the SNR of 44 \pm 4 is high enough to provide relevant signal information and shape, especially considering the 12-fold difference in the electrode size. Moreover, ECG can be recorded in a less sophisticated way by placing two tattoos on opposite hands (e.g., forearms) and a single reference electrode near a bone (e.g., elbow). Such data are shown in Figure S8, featuring a clear and high amplitude ECG signal having the essential large P, Q, R, S, and T domains.

EMG is a distinct, powerful, and useful electrical signal that corresponds to the muscles' physical contractions within the body. 41 When a pair of electrodes biased in a differential manner are placed over a muscle, the muscular contractions will generate a net electrical potential. Typically, the larger the distance between the two electrodes, the larger the differential signal recorded from the pair. In order to record useful EMG signals, we placed a pair of Pt-TMD tattoos on a forearm and another pair of tattoos on a bicep, along with the pairs of Ag/AgCl electrodes for direct comparison (see schematics on Figure 5d). During a series of forearm contractions (mechanical expander) and bicep curls, we clearly distinguished those movements via simple monitoring of the EMG activity and the signal's power. One can see that the signal power from gel electrodes is higher compared to that for Pt-TMDs, which is due to 12 times larger electrode area as well as the almost 5 times higher spacing between the electrodes. Nonetheless, as it can be seen from Figure 5d for PtTe₂ and Figure S9 for PtSe₂, we are able to optimally recognize both: movements of the forearm and bicep as well as differentiate between them. On the brighter side, Pt-TMD electrodes feature lower noise, essentially displaying higher signal specificity, equalizing the performance. The higher signal specificity of Pt-TMD tattoos here relates to superior adhesion to skin. Mechanical movements push the large gel

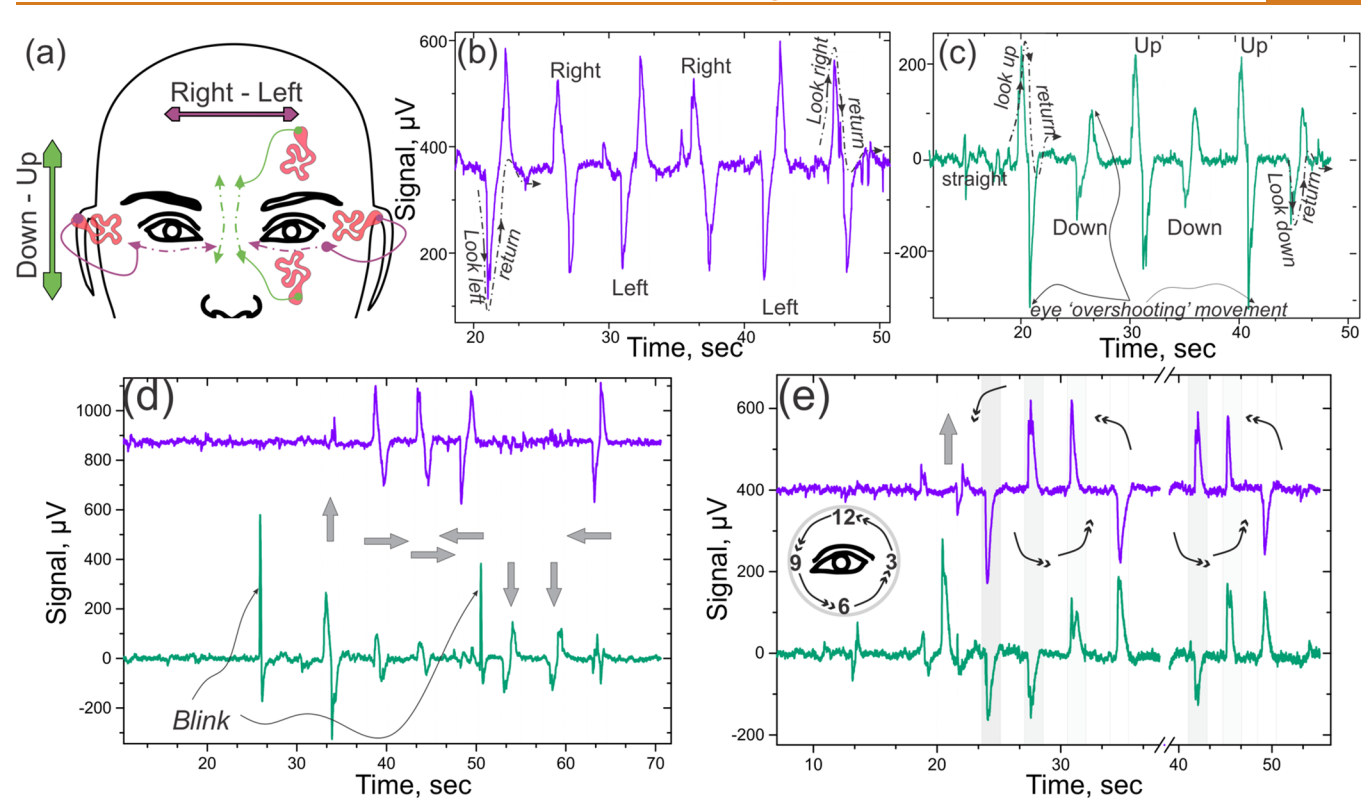


Figure 6. (a) Schematic of the electrode placement for the EOG experiments performed with PtTe₂ tattoos. (b) EOG signals corresponding to the differential channel recording left—right eye movements (violet here and after). (c) EOG signals corresponding to the differential channel recording up—down eye movements (green here and after). (d) EOG recordings from both channels when the subject is gazing up, right, right, left, down, down, and left consecutively with 5 s dwell time. (e) EOG recordings from both channels when the subject is looking counterclockwise with four distinct stops: at "12", "9", "6", and "3" o'clock. Straight and angular arrows in (d,e) correspondingly show the direction of sight.

electrodes to move physically, creating motion artifacts, that contribute to higher noise. As can be seen from the timetrace of consecutive bicep and forearm movements (see Figure 5d), often, the muscular movement associated with a bicep curl also results in slight forearm muscle contractions, which is always picked up by the large Ag/AgCl gel electrodes. These nonspecific signals usually obstruct from making clear and decisive interfacing, and as it is evident from the results provided, smaller Pt-TMD tattoos suffer much less from this problem.

The low contact electrode-skin impedance displayed by Pt-TMDs is essential for most electrophysiological measurements but especially for EEG. EEG signals are electrical signals associated with the ever-active electrical activities inside the brain. 42,43 There is a broad scientific community working on EEG and its applications, mostly studying the correlations between EEG signals and the underlying brain functions. Developing a tattoo system that can be used for EEG recordings (a) reliably, (b) with intimate contact and signal quality, and (c) reusable is a high-impact task. To measure EEG signals, a couple of Pt-TMD tattoos were placed on the subject's forehead, precisely onto the Fp1 and Fp2 locations, 44 and sampled separately with a common ground electrode connected to an earlobe. The EEG recordings were typically collected over a period of 120-240 s and featured specific patterns of subjects' activities—their eyes being open or closed. After applying the short-time Fourier transformation (STFT) onto the recorded signals, the output spectrogram, as shown in Figure 5e, reveals the heatmap of signal frequency components and their power levels (in dB), distributed over the entire timetrace. It is well-known that EEG, recorded from the forehead, should show prevailing α waves (8–13 Hz) when the subject's eyes are closed, especially at the Fp1 and Fp2 locations. As seen from Figure 5e and Figure S12, the spectrogram patterns pick up the α waves when "eyes closed" with PtTe₂ and PtSe₂ tattoos and Ag/AgCl gel electrodes. To specifically show the statistical presence of α rhythms, we have averaged and plotted the spectral power density from gel, PtSe₂, and PtTe₂ electrodes with open and closed eye intervals. As seen from the fast Fourier transform (FFT) data (see Figure S13), there is a significant power density peak around 8–13 Hz that corresponds to the α waves when "eyes closed", yet the peak is absent in the case of "eyes open".

To showcase a human-machine interface enabled by the Pt-TMD tattoos, we measured electrical signals associated with the eye movements, 46 which could easily be later channeled into a computer, robot, or machine. 47,48 EOGs are very similar to the EMG signals but are associated with the differences in polarization of the eye's cornea and retina.⁴⁹ To record EOG signals, we have placed four Pt-TMDs on a subject's face: one pair goes above and below the left eye, one tattoo on the left side of the left eye, and the last tattoo on the right side of the right eye (see Figure 6a for details). The tattoos placed on the sides of the eyes are connected differentially into a single channel, and the electrodes above and below the left eye are connected differentially to the other channel. When the subject is looking into a particular direction, specific cornea-retina depolarization events create electric potential differences associated with the movement. As seen from the timetrace recordings (see Figure 6b), gazing left and right results in the distinct change of the appropriate channel's EOG signal. Similarly, gazing up and down results in a specific pattern recorded by another pair of electrodes (see Figure 6c). The EOG signals, as shown in Figure S14, for example, are very sharp and associated with rapid and repetitive eye movements without a distinct baseline. When slower gazing experiments are performed, a clear differentiation can be made between various gazing patterns (e.g., up-down, up-center, left-center, center-right, etc.). There is, however, a certain "overshoot" signal that can be seen in some recordings (see Figure 6b,c) when the eyes are returning from a peripheral into straight positions. However, these "overshoots" are directional and help distinguish the change of sight direction in dynamics. Figure 6d shows the results of an elaborate, nonroutine experiment when the subject was instructed to look into the direction as conducted by the experimenter, online and without any warning. It is visible that the patterns for looking down, up, left, and right can be discretely identified. Such a pattern is readily distinguishable, allowing us to differentiate between arbitrary directions. Eye blinks do cause some troubles and create certain events, mainly in the up-down channel, yet they can be later postprocessed and removed.⁵⁰

In the final EOG experiment, the subject was instructed to perform more sophisticated eye movements that are not just fixed to one degree of freedom (straight horizontal or straight vertical) as before. Here, the subject performed circular eye movements (like looking over a watch) counterclockwise with four distinct stops: at 12, 9, 6, and 3 o'clock positions. Astonishingly, those movements resemble a combination of the aforementioned two-degree movements. For example, when moving from 12 to 9, the recorded signal pattern is a combination of the signals corresponding to "left" and "down" (see Figure 6e for details). The results clearly indicate that the TMD tattoos can constitute a technology that does advanced eye-tracking for human—machine interfaces.

In addition to recording human electrophysiological signals, the Pt-TMD tattoos can also measure skin temperature. Continuous and precise human body temperature monitoring is an important feature for next-generation wearables. Tracking and monitoring the body core temperature changes is essential to provide an early response to possible viral infection or disease. With Pt-TMD tattoos, we have found the task of temperature monitoring very intriguing. Here, the two dichalcogenides of choice turned out to have opposite signs of temperature electrical coefficients. The TECs were evaluated by measuring the tattoo's resistance while changing the environment's temperature and having a commercial thermocouple to control the actual surface temperature. As one can see from Figures S15 and S16, the TEC of PtTe₂ has a positive sign, and the α coefficient ranges between 0.0004 and 0.0020, whereas PtSe2 features a negative TEC with the coefficient between -0.0010 and -0.0013. Here, PtTe₂ behaves like the majority of metals and increases its resistance with increased temperature. In PtSe2, however, the resistance decreases with increased temperature featuring negative TEC, which is unexpected, as the PtSe₂ material used for this experiment is a highly conductive semimetal. Furthermore, the overall temperature response is linear over a broad temperature range tested, from 15 °C and beyond 60 °C, which is well within the human body temperature range. To validate Pt-TMD tattoos for measuring real-time skin temperature, we placed them onto a subject's forearm with a thermocouple nearby. After approximately 2 min of control measurement, an ice bag was brought in contact with the skin,

held for a couple of minutes, then removed. The timetrace of PtSe₂'s resistance change and thermocouple's response can be seen in Figure S15b. As expected, upon being cooled, PtSe₂ resistance had increased. Moreover, it is evident that there is no lag in the response in comparison to commercial thermocouples; that is, the slow decay of changes in resistance visible in Figure S15b are associated directly with the temperature profile and not to the materials' properties.

CONCLUSIONS

In conclusion, we present in this work high-quality advanced electronic tattoos made of Pt-TMDs, namely, PtSe₂ and PtTe₂ that can used be for wearable bioelectronic applications. Both PtSe₂ and PtTe₂, particularly the latter, possess high conductivity desirable for wearable and implantable electrodes. In terms of electrode-skin impedance, a figure-of-merit for wearable electrode systems, Pt-TMDs outperform graphenebased electronic tattoos, state-of-the-art noble metal tattoos, and medical-grade gel electrodes (see full comparison at Supplementary Table S1). The tattoos are ultrathin, form intimate contact with skin, and can be made via direct temperature conversion of Pt on top of polymer substrates. Brainwayes, heart function, muscle activity, skin temperature, and even eyetracking are shown to be accurately captured by means of Pt-TMD electronic tattoos. The eye-tracking is of particular interest as it applies to wearable human—machine interfaces. We have successfully used two of the pairs of PtTe₂ and PtSe₂ tattoos built on Kapton film for all electrophysiology modalities reported in this work, including EEG, EMG, ECG, and EOG, highlighting their reusability and versatility.

METHODS

PtSe2 and **PtTe2 Growth.** The PtSe2 and PtTe2 layers were grown on the substrates of choice (SiO_2/Si , Kapton) using a two-step thermal-assisted conversion process. Electron beam deposition (Temescal) was used to deposit Pt films of desired thickness at a rate of 0.1 Å/s on the substrates. The Pt-covered substrates are then placed in the middle zone of a CVD tube furnace with alumina boat containing tellurium (Te) or selenium (Se) placed at the upstream region for tellurization or selenization to obtain PtTe2 or PtSe2 layers, respectively. The CVD tube is pumped down to a low pressure of 25 mTorr followed by purging with argon (Ar) gas at a high flow rate to remove the moisture and residual gases. For both PtTe2 and PtSe2, the furnace is heated to the growth temperature of 400 °C and held there for 50 min under a constant flow of Ar. The furnace is left to cool to room temperature naturally.

Optical Transmittance and Water Contact Angle Measurements. The optical transmittance of $PtSe_2$ and $PtTe_2$ samples directly grown on optically transparent willow glass were characterized using ultraviolet—visible (UV—vis) spectroscopy (Cary WinUV spectrophotometer) in the wavelength range of 200–800 nm. Water contact angle measurements on SiO_2/Si substrates were carried out using a goniometer (Rame Hart 90-U3-PRO), and the same water volume was used to ensure uniformity of all measurements.

Raman and XPS Characterization. X-ray photoelectron spectroscopy characterization of $PtSe_2$ and $PtTe_2$ samples was carried out using a Thermo VG Scientific K- α system under ultrahigh vacuum conditions. The system has an energy resolution of $\sim\!0.5$ eV and 100 W X-ray spot of 400 μm^2 . The binding energy of C 1s, 284.5 eV, is used to calibrate the XPS peaks, and Voigt functions are used for the peak fitting. Raman spectroscopy was performed in a Renishaw inVia micro-Raman system. The excitation wavelength of 532 nm with an incident beam power of $\sim\!1$ mW and exposure time of 10 s is used for Raman measurement.

Electrophysiology Data Collection. The EEG, EMG, ECG, and EOG signals were all recorded *via* the Ganglion Open-BCI board. ⁵¹

The board is a low-cost yet effective tool. The board itself is approximately 8×8 cm in size and powered by a 3.3 V-6 V battery, and has a BLE module on board, making it freely portable. The Ganglion board features four high-impedance differential inputs. The channels are sampled separately, using a maximum of four pairs of electrodes (one pair for each channel) for monitoring EMG, EOG, and ECG. In order to record EEG, the differential inputs can be connected to a single reference electrode, which is typically located on the earlobe. The board records data with a sampling rate of 200 Hz.

Skin Impedance Measurements. The electrode—skin impedance is measured *via* a Hioki LCR meter IM3536, which has a max frequency sweep range between 4 Hz and up to 8 MHz. For our study, however, we narrowed the measurement window down to 10 Hz—1 MHz. The measurements are performed in the constant voltage mode with 50 mV AC amplitude, without DC bias. Each data point is measured four times and averaged instrumentally. The frequency sweep is usually performed three times, with each sweep taking approximately 90 s and 10 s delay between sweeps. The measured values correspond to the electrode—skin impedance as the tissue's bioimpedance is much smaller when compared to the typical electrode—skin impedance. ⁵² During the measurements, the skin moisture was not specifically monitored, neither was it manually induced or changed during the experiments. The characterization experiments were performed on one subject; hence any subject-to-subject performance variability is diminished.

Electrophysiology Data Analysis. The data processing was performed with MATLAB, and the designed code is available on request. Raw ECG, EMG, ECG, and EOG data, as acquired by the OpenBCI board, were utilized for analysis. The recordings are stored in four separate channels, and the sample values are arranged in the form of vectors. The raw signals have a significant noise in the 60 Hz frequency region, and hence an appropriate 60 Hz notch filter was implemented before any further processing. To analyze the ECG signals, we performed a peak finding algorithm. From each peak found, we extracted its amplitude, which was further averaged to get the average signal (S) value. In order to find the noise, we extracted n regions of 200 ms duration between two spikes and found the median absolute deviation (MAD) of that timetrace. Twice MAD was considered the noise (N). The signal-to-noise ratio is calculated accordingly by dividing signal amplitude by noise level. The EEG recordings were typically in the range of 120-240 s long. Two out of four OpenBCI channels correspond to the Fp1 and Fp2 locations' EEG measurements, whereas the other two channels were turned off. First, a 60 Hz notch filter was implemented, followed by linear detrending to remove the baseline. Also, a low-pass filter with a cutoff frequency of 50 Hz was designed and implemented to further cutoff the high-frequency noise. As a crucial part of this analysis, STFT was implemented with the Hamming window of 128 sample length and the FFT length of 512 samples. The STFT output as a matrix consisting of frequency and time samples, the corresponding Fourier coefficients, and the power spectral densities in dB units were stored separately and utilized for further plotting. The formulas utilized here can be found elsewhere.

Electrical Impedance Spectroscopy. We utilized the Autolab PGSTAT 128N potentiostat with NOVA software for data acquisition and preliminary processing for EIS characterization. A 1× phosphate-buffered saline solution was used as the standard electrolyte for the measurements, Ag/AgCl as a reference electrode, Pt wire as a counter electrode, and the material of interest (Pt, PtSe₂, PtTe₂, and Au) was connected as the working electrode. Appropriate frequency ranges for the plots were set, and measurements were taken. Areas of 20, 24, 30, 35, and 40 mm² of the 2D TMD and reference materials were utilized in the EIS measurement runs.

Temporary Tattoo Fabrication. A layer of PMMA (950 A4) is spin-coated on top of Pt-TMD/SiO₂/Si at the rate of ~2500 rpm for 60 s and hard-baked at 200 °C for 20 min, resulting in ~200 nm thick support layer. A TRT film (120 °C release temperature, 3195MS Nitto Denko Revalpha) is carefully placed in contact with the PMMA, avoiding bubble formation. It is important to note here that, prior to the Pt evaporation and TMD growth, the SiO₂/Si surface was treated with oxygen plasma for 5 min to improve the surface's hydrophilicity and demote the material's adhesion. The TRT/PMMA/Pt-TMD/SiO₂/Si

stack is then placed into a water bath for 5–10 min for soaking. Then, the TRT/PMMA/Pt-TMD is carefully mechanically delaminated from the surface of SiO₂/Si. The process works best in water due to the specific interface of Pt-TMD and SiO₂: the TMDs are hydrophobic, whereas the SiO₂ is hydrophilic; therefore, upon peeling off, the water propagates into the bulk of the film, coats SiO₂/Si, and pushes the TMD out, assisting in the separation. When the TRT/PMMA/Pt-TMD is fully delaminated, it is dried slowly at room temperature. Before Pt-TMD is transferred onto tattoo paper, the paper itself must be prepared. The tattoo paper comes with a thin layer of poly(vinyl alcohol) (PVA) on top, which must be removed. It is done by simply soaking the paper in water for 30 s and picking up the partially dissolved PVA with tweezers. When the PVA is removed, the tattoo paper can be dried out by quick N2 gun assisted drying and 10 min dry under ambient conditions. The TRT/PMMA/Pt-TMD is then brought in contact with the tattoo paper and placed on a hot plate at room temperature. The hot plate is then slowly heated to 120 $^{\circ}\text{C}$ when the TRT is delaminated by itself, leaving the PMMA/Pt-TMD on top of the tattoo paper. In order to flip the PMMA/Pt-TMD to result in Pt-TMD facing up, it is simply flipped onto another tattoo paper. The material is then shaped into an arbitrary pattern with resolution down to 500 µm via a mechanical plotter, Silhouette Cameo (see Supplementary Video S2 for details).⁵ To transfer onto skin, the tattoo is soaked in water again, causing the paper to be slippery, allowing the transfer, and brought in contact with human skin. Sliding away the tattoo paper, Pt-TMD tattoo will stay on the skin; see Supplementary Video S3 for details. After the measurements, the tattoos can be very easily removed by gentle picking up via kind removal silicone tape for disposal (see Supplementary Video S4).

Fabrication of Soft Tapes and Ecoflex Slides. In order to yield the thinnest possible electrical contacts that at the same time adhere to the skin, we utilized a 10 μ m thick adhesive tape (Iwatani, ISR-BSMK10G) and evaporated a metal stack (Ni/Au, 10/90 nm) on top of it. The tape is supported by the PET backing layer, which is delaminated from PET right before placing the tape onto the skin.

To make the skin-resembling surface for resistance measurements, we coated glass slides with a thick (2–4 mm) layer of Ecoflex 00-30, which was cured at room temperature for 48 h.

Experiments on Human Subjects. All experiments were conducted under the Institutional Review Board's approval at the University of Texas at Austin (protocol number: 2018-06-0058).

ASSOCIATED CONTENT

Supporting Information

The Supporting Information is available free of charge at https://pubs.acs.org/doi/10.1021/acsnano.0c08689.

Additional figures as described in the text (PDF) Mechanical stability of Pt-TMD tattoos (MP4) Mechanical cutting process of Pt-TMD tattoos (MP4) Detailed procedure of tattoo placement on the skin (MP4) Tattoo removal (MP4)

AUTHOR INFORMATION

Corresponding Author

Dmitry Kireev — Department of Electrical and Computer Engineering, The University of Texas at Austin, Austin, Texas 78758, United States; Microelectronics Research Center, The University of Texas at Austin, Austin, Texas 78758, United States; orcid.org/0000-0003-1499-5435; Phone: +1-737-230-5319; Email: d.kireev@utexas.edu, kirdmitry@gmail.com

Authors

Emmanuel Okogbue — NanoScience Technology Center, University of Central Florida, Orlando, Florida 32826, United States; Department of Electrical and Computer Engineering,

- University of Central Florida, Orlando, Florida 32816, United States
- RT Jayanth Department of Electrical and Computer Engineering, The University of Texas at Austin, Austin, Texas 78758, United States
- Tae-Jun Ko NanoScience Technology Center, University of Central Florida, Orlando, Florida 32826, United States
- Yeonwoong Jung NanoScience Technology Center, University of Central Florida, Orlando, Florida 32826, United States; Department of Electrical and Computer Engineering and Department of Materials Science and Engineering, University of Central Florida, Orlando, Florida 32816, United States; orcid.org/0000-0001-6042-5551
- Deji Akinwande Department of Electrical and Computer Engineering, The University of Texas at Austin, Austin, Texas 78758, United States; Microelectronics Research Center and Texas Materials Institute, The University of Texas at Austin, Austin, Texas 78758, United States; orcid.org/0000-0001-7133-5586

Complete contact information is available at: https://pubs.acs.org/10.1021/acsnano.0c08689

Notes

The authors declare no competing financial interest.

ACKNOWLEDGMENTS

The work was supported in part by the Office of Naval Research Grant No. N00014-18-1-2706, the Temple Foundation Endowed Professorship, the National Science Foundation (CMMI-1728390), and the Creative Materials Discovery Program through the National Research Foundation of Korea (NRF) (NRF-2019M3D1A1069793).

REFERENCES

- (1) Zhou, J.; Lin, J.; Huang, X.; Zhou, Y.; Chen, Y.; Xia, J.; Wang, H.; Xie, Y.; Yu, H.; Lei, J.; Wu, D.; Liu, F.; Fu, Q.; Zeng, Q.; Hsu, C. H.; Yang, C.; Lu, L.; Yu, T.; Shen, Z.; et al. A Library of Atomically Thin Metal Chalcogenides. *Nature* **2018**, *556* (7701), *355*–359.
- (2) Manzeli, S.; Ovchinnikov, D.; Pasquier, D.; Yazyev, O. V.; Kis, A. 2D Transition Metal Dichalcogenides. *Nat. Rev. Mater.* **2017**, *2*, 17033.
- (3) Kang, J.; Zhang, L.; Wei, S. H. A Unified Understanding of the Thickness-Dependent Bandgap Transition in Hexagonal Two-Dimensional Semiconductors. *J. Phys. Chem. Lett.* **2016**, 7 (4), 597–602.
- (4) Villaos, R. A. B.; Crisostomo, C. P.; Huang, Z. Q.; Huang, S. M.; Padama, A. A. B.; Albao, M. A.; Lin, H.; Chuang, F. C. Thickness Dependent Electronic Properties of Pt Dichalcogenides. *npj 2D Mater. Appl.* **2019**, 3 (1), 1–8.
- (5) Pang, Y.; Yang, Z.; Yang, Y.; Ren, T. L. Wearable Electronics Based on 2D Materials for Human Physiological Information Detection. *Small* **2020**, *16* (15), 1901124.
- (6) Lacour, S. P.; Courtine, G.; Guck, J. Materials and Technologies for Soft Implantable Neuroprostheses. *Nat. Rev. Mater.* **2016**, *1*, 16063.
- (7) Lee, J.; Shin, J.-H.; Lee, G.-H.; Lee, C.-H. Two-Dimensional Semiconductor Optoelectronics Based on van der Waals Heterostructures. *Nanomaterials* **2016**, *6* (11), 193.
- (8) Pourbaix, M. J. N.; Van Muylder, J.; de Zoubov, N. Electrochemical Properties of the Platinum Metals. *Platinum Met. Rev.* **1959**, 3 (2), 47–53.
- (9) Greeley, J.; Stephens, I. E. L.; Bondarenko, A. S.; Johansson, T. P.; Hansen, H. A.; Jaramillo, T. F.; Rossmeisl, J.; Chorkendorff, I.; Nørskov, J. K. Alloys of Platinum and Early Transition Metals as Oxygen Reduction Electrocatalysts. *Nat. Chem.* **2009**, *1* (7), 552–556. (10) Geninatti, T.; Bruno, G.; Barile, B.; Hood, R. L.; Farina, M.; Schmulen, J.; Canavese, G.; Grattoni, A. Impedance Characterization,

- Degradation, and *in Vitro* Biocompatibility for Platinum Electrodes on BioMEMS. *Biomed. Microdevices* **2015**, *17* (1), 1–11.
- (11) Zhao, Y.; Qiao, J.; Yu, Z.; Yu, P.; Xu, K.; Lau, S. P.; Zhou, W.; Liu, Z.; Wang, X.; Ji, W.; Chai, Y. High-Electron-Mobility and Air-Stable 2D Layered PtSe2 FETs. *Adv. Mater.* **2017**, *29* (5), 1604230.
- (12) Ciarrocchi, A.; Avsar, A.; Ovchinnikov, D.; Kis, A. Thickness-Modulated Metal-to-Semiconductor Transformation in a Transition Metal Dichalcogenide. *Nat. Commun.* **2018**, *9* (1), 1–6.
- (13) Yim, C.; Lee, K.; McEvoy, N.; O'Brien, M.; Riazimehr, S.; Berner, N. C.; Cullen, C. P.; Kotakoski, J.; Meyer, J. C.; Lemme, M. C.; Duesberg, G. S. High-Performance Hybrid Electronic Devices from Layered PtSe2 Films Grown at Low Temperature. *ACS Nano* **2016**, *10* (10), 9550–9558.
- (14) Okogbue, E.; Han, S. S.; Ko, T.-J.; Chung, H.-S.; Ma, J.; Shawkat, M. S.; Kim, J. H.; Kim, J. H.; Ji, E.; Oh, K. H.; Zhai, L.; Lee, G.-H.; Jung, Y. Multifunctional Two-Dimensional PtSe2-Layer Kirigami Conductors with 2000% Stretchability and Metallic-to-Semiconducting Tunability. *Nano Lett.* 2019, 19 (11), 7598–7607.
- (15) Han, S. S.; Kim, J. H.; Noh, C.; Kim, J. H.; Ji, E.; Kwon, J.; Yu, S. M.; Ko, T. J.; Okogbue, E.; Oh, K. H.; Chung, H. S.; Jung, Y.; Lee, G. H.; Jung, Y. Horizontal-To-Vertical Transition of 2D Layer Orientation in Low-Temperature Chemical Vapor Deposition-Grown PtSe2 and Its Influences on Electrical Properties and Device Applications. *ACS Appl. Mater. Interfaces* **2019**, *11* (14), 13598–13607.
- (16) Guo, G. Y.; Liang, W. Y. The Electronic Structures of Platinum Dichalcogenides: PtS2, PtSe2 and PtTe2. *J. Phys. C: Solid State Phys.* **1986**, 19 (7), 995–1008.
- (17) Soled, S.; Wold, A.; Gorochov, O. Crystal Growth and Characterization of Platinum Ditelluride. *Mater. Res. Bull.* **1975**, *10* (8), 831–835.
- (18) Yan, M.; Huang, H.; Zhang, K.; Wang, E.; Yao, W.; Deng, K.; Wan, G.; Zhang, H.; Arita, M.; Yang, H.; Sun, Z.; Yao, H.; Wu, Y.; Fan, S.; Duan, W.; Zhou, S. Lorentz-Violating Type-II Dirac Fermions in Transition Metal Dichalcogenide PtTe2. *Nat. Commun.* **2017**, *8* (1), 1–6
- (19) Okogbue, E.; Ko, T.-J.; Han, S. S.; Shawkat, M. S.; Wang, M.; Chung, H.-S.; Oh, K. H.; Jung, Y. Wafer-Scale 2D PtTe2 Layers for High-Efficiency Mechanically Flexible Electro-Thermal Smart Window Applications. *Nanoscale* **2020**, *12*, 10647.
- (20) Wang, M.; Ko, T.-J.; Shawkat, M. S.; Han, S. S.; Okogbue, E.; Chung, H.-S.; Bae, T.-S.; Sattar, S.; Gil, J.; Noh, C.; Oh, K. H.; Jung, Y.; Larsson, J. A.; Jung, Y. Wafer-Scale Growth of 2D PtTe2 with Layer Orientation Tunable High Electrical Conductivity and Superior Hydrophobicity. ACS Appl. Mater. Interfaces 2020, 12 (9), 10839–10851.
- (21) Rosli, N. F.; Mayorga-Martinez, C. C.; Latiff, N. M.; Rohaizad, N.; Sofer, Z.; Fisher, A. C.; Pumera, M. Layered PtTe2Matches Electrocatalytic Performance of Pt/C for Oxygen Reduction Reaction with Significantly Lower Toxicity. ACS Sustainable Chem. Eng. 2018, 6 (6), 7432–7441.
- (22) Kabiri Ameri, S.; Ho, R.; Jang, H.; Tao, L.; Wang, Y.; Wang, L.; Schnyer, D. M.; Akinwande, D.; Lu, N. Graphene Electronic Tattoo Sensors. *ACS Nano* **2017**, *11* (8), 7634–7641.
- (23) Politano, A.; Chiarello, G.; Kuo, C.-N.; Lue, C. S.; Edla, R.; Torelli, P.; Pellegrini, V.; Boukhvalov, D. W. Tailoring the Surface Chemical Reactivity of Transition-Metal Dichalcogenide PtTe2 Crystals. *Adv. Funct. Mater.* **2018**, 28 (15), 1706504.
- (24) Sajjad, M.; Singh, N.; Schwingenschlögl, U. Strongly Bound Excitons in Monolayer PtS2 and PtSe2. *Appl. Phys. Lett.* **2018**, *112* (4), 043101.
- (25) Fu, L.; Hu, D.; Mendes, R. G.; Rummeli, M. H.; Dai, Q.; Wu, B.; Fu, L.; Liu, Y. Highly Organized Epitaxy of Dirac Semimetallic PtTe2 Crystals with Extrahigh Conductivity and Visible Surface Plasmons at Edges. *ACS Nano* **2018**, *12* (9), 9405–9411.
- (26) Hao, S.; Zeng, J.; Xu, T.; Cong, X.; Wang, C.; Wu, C.; Wang, Y.; Liu, X.; Cao, T.; Su, G.; Jia, L.; Wu, Z.; Lin, Q.; Zhang, L.; Yan, S.; Guo, M.; Wang, Z.; Tan, P.; Sun, L.; Ni, Z.; Liang, S.-J.; Cui, X.; Miao, F.; et al. Low-Temperature Eutectic Synthesis of PtTe2 with Weak

- Antilocalization and Controlled Layer Thinning. Adv. Funct. Mater. 2018, 28 (36), 1803746.
- (27) Shi, J.; Huan, Y.; Hong, M.; Xu, R.; Yang, P.; Zhang, Z.; Zou, X.; Zhang, Y. Chemical Vapor Deposition Grown Large-Scale Atomically Thin Platinum Diselenide with Semimetal-Semiconductor Transition. *ACS Nano* **2019**, *13* (7), 8442–8451.
- (28) Ko, T.-J.; Han, S. S.; Okogbue, E.; Shawkat, M. S.; Wang, M.; Ma, J.; Bae, T.-S.; Hafiz, S. B.; Ko, D.-K.; Chung, H.-S.; Oh, K. H.; Jung, Y. Wafer-Scale 2D PtTe2 Layers-Enabled Kirigami Heaters with Superior Mechanical Stretchability and Electro-Thermal Responsiveness. *Appl. Mater. Today* **2020**, *20*, 100718.
- (29) Cho, M. C.; Kim, J. Y.; Cho, S. H. A Bio-Impedance Measurement System for Portable Monitoring of Heart Rate and Pulse Wave Velocity Using Small Body Area. *Proc. IEEE Int. Symp. Circuits Syst.* **2009**, *1*, 3106–3109.
- (30) Li, G.; Wang, S.; Duan, Y. Y. Towards Gel-Free Electrodes: A Systematic Study of Electrode-Skin Impedance. *Sens. Actuators, B* **2017**, 241, 1244–1255.
- (31) Ferrari, L. M.; Sudha, S.; Tarantino, S.; Esposti, R.; Bolzoni, F.; Cavallari, P.; Cipriani, C.; Mattoli, V.; Greco, F. Ultraconformable Temporary Tattoo Electrodes for Electrophysiology. *Adv. Sci.* **2018**, 5 (3), 1700771.
- (32) Gandhi, N.; Khe, C.; Chung, D.; Chi, Y. M.; Cauwenberghs, G. Properties of Dry and Non-Contact Electrodes for Wearable Physiological Sensors. *Proc. 2011 Int. Conf. Body Sens. Networks, BSN 2011* **2011**, 107–112.
- (33) Sel, K.; Ibrahim, B.; Jafari, R. ImpediBands: Body Coupled Bio-Impedance Patches for Physiological Sensing Proof of Concept. *IEEE Trans. Biomed. Circuits Syst.* **2020**, *14*, 757.
- (34) Han, S. S.; Ko, T.-J.; Yoo, C.; Shawkat, M. S.; Li, H.; Kim, B. K.; Hong, W.-K.; Bae, T.-S.; Chung, H.-S.; Oh, K. H.; Jung, Y. Automated Assembly of Wafer-Scale 2D TMD Heterostructures of Arbitrary Layer Orientation and Stacking Sequence Using Water Dissoluble Salt Substrates. *Nano Lett.* **2020**, *20* (5), 3925–3934.
- (35) Beasley, C. Basics of Electrochemical Impedance Spectroscopy. *Webinar EIS Batter.* **2015**, DOI: 10.1152/ajpregu.00432.2003.
- (36) Jeong, J. W.; Yeo, W. H.; Akhtar, A.; Norton, J. J. S.; Kwack, Y. J.; Li, S.; Jung, S. Y.; Su, Y.; Lee, W.; Xia, J.; Cheng, H.; Huang, Y.; Choi, W. S.; Bretl, T.; Rogers, J. A. Materials and Optimized Designs for Human-Machine Interfaces *via* Epidermal Electronics. *Adv. Mater.* **2013**, 25 (47), 6839–6846.
- (37) Sel, K.; Kireev, D.; Brown, A.; Ibrahim, B.; Akinwande, D.; Jafari, R. Electrical Characterization of Graphene-Based e-Tattoos for Bio-Impedance-Based Physiological Sensing. *BioCAS* 2019 *Biomed. Circuits Syst. Conf. Proc.* 2019, 1–4.
- (38) Becq, G.; Bienkowski, G.; Diard, J.-P.; Villard, C. About MEA Impedance Measurement and Analysis. 6th International Meeting on Substrate-Integrated Micro Electrode arrays, July 2008, Reutlingen, Germany; pp 277–278.
- (39) Kireev, D.; Offenhäusser, A. Graphene & Two-Dimensional Devices for Bioelectronics and Neuroprosthetics. 2D Mater. 2018, 5 (4), 042004.
- (40) Bjerregaard, P.; Gussak, I. Naming of the Waves in the ECG With a Brief Account of Their Genesis. *Circulation* **1999**, *100* (25), 1937–1942.
- (41) Sadikoglu, F.; Kavalcioglu, C.; Dagman, B. Electromyogram (EMG) Signal Detection, Classification of EMG Signals and Diagnosis of Neuropathy Muscle Disease. *Procedia Comput. Sci.* **2017**, *120*, 422–429
- (42) Vaid, S.; Singh, P.; Kaur, C. EEG Signal Analysis for BCI Interface: A Review. *Int. Conf. Adv. Comput. Commun. Technol. ACCT* **2015**, 143–147.
- (43) Vidal, F.; Burle, B.; Spieser, L.; Carbonnell, L.; Meckler, C.; Casini, L.; Hasbroucq, T. Linking EEG Signals, Brain Functions and Mental Operations: Advantages of the Laplacian Transformation. *Int. J. Psychophysiol.* **2015**, *97* (3), 221–232.
- (44) Oostenveld, R.; Praamstra, P. The Five Percent Electrode System for High-Resolution EEG and ERP Measurements. *Clin. Neurophysiol.* **2001**, *112* (4), 713–719.

- (45) Li, L. The Differences among Eyes-Closed, Eyes-Open and Attention States: An EEG Study. 2010 6th Int. Conf. Wirel. Commun. Netw. Mob. Comput. WiCOM 2010 No. Nsfc 30800242, 2010; DOI: 10.1109/WICOM.2010.5600726.
- (46) Bulling, A.; Ward, J. A.; Gellersen, H.; Tröster, G. Eye Movement Analysis for Activity Recognition Using Electrooculography. *IEEE Trans. Pattern Anal. Mach. Intell.* **2011**, 33 (4), 741–753.
- (47) Usakli, A. B.; Gurkan, S.; Aloise, F.; Vecchiato, G.; Babiloni, F. On the Use of Electrooculogram for Efficient Human Computer Interfaces. *Comput. Intell. Neurosci.* **2010**, 2010, 1–5.
- (48) Kim, D. Y.; Han, C. H.; Im, C. H. Development of an Electrooculogram-Based Human-Computer Interface Using Involuntary Eye Movement by Spatially Rotating Sound for Communication of Locked-In Patients. *Sci. Rep.* **2018**, *8* (1), 1–10.
- (49) Barea Navarro, R.; Boquete Vázquez, L.; López Guillén, E. EOG-Based Wheelchair Control. In *Smart Wheelchairs and Brain-Computer Interfaces*; Diez, P., Ed.; Academic Press, 2018; pp 381–403.
- (50) Gao, J. F.; Yang, Y.; Lin, P.; Wang, P.; Zheng, C. X. Automatic Removal of Eye-Movement and Blink Artifacts from EEG Signals. *Brain Topogr* **2010**, 23 (1), 105–114.
- (51) OpenBCI. Ganglion Getting Started Guide; https://docs.openbci.com/docs/01GettingStarted/01-Boards/GanglionGS.
- (52) Ibrahim, B.; McMurray, J.; Jafari, A. R. A Wrist-Worn Strap with an Array of Electrodes for Robust Physiological Sensing. *Proc. Annu. Int. Conf. IEEE Eng. Med. Biol. Soc. EMBS* **2018**, 4313–4317.
- (53) Zahniser, D. J.; Brenner, J. F. Signals and Systems. *Cytometry*; Oppenheim, A.V., Willsky, A.S., Young, I. T., Eds.; Prentice-Hall: Englewood Cliffs, NJ, 1983.
- (\$\tilde{5}4\$) Yang, S.; Chen, Y.-C.; Nicolini, L.; Pasupathy, P.; Sacks, J.; Su, B.; Yang, R.; Sanchez, D.; Chang, Y.-F.; Wang, P.; Schnyer, D.; Neikirk, D.; Lu, N. Cut-And-Paste" Manufacture of Multiparametric Epidermal Sensor Systems. *Adv. Mater.* **2015**, *27* (41), 6423–6430.